

Current pulse generator: A circuit for programming RRAM in current mode

B. Zhang,¹ P. Gibertini,¹ M. Akbari,¹ and E. Covi¹

*Zernike Institute of Advanced Materials & CogniGron, University of Groningen
Nijenborgh 3, 9747 AG Groningen, Netherlands*

(Dated: 2 March 2026)

Switching uniformity, as a major challenge, hinders the practical implementation of Resistive random access memory (RRAM) in memory application. Operating RRAM in current mode, is proposed as an efficient method to improve programming schemes accuracy within the finite readout window. In this article, we demonstrate a current generator circuit to perform current programming on RRAM. Current mirror topology is used in our circuit to convert an external pulse voltage into a pulse current fed to RRAM directly with an amplitude equivalent with the DC reference current. The targeting ranges of RRAM's programming current are up to 400 μA and, in that case, our proposed circuit achieved minimum current mismatch of 1%.

I. INTRODUCTION

RRAM technology has received widespread attention for the potential as a promising future non-volatile memory (NVM). Its non-volatile switching behavior ensures good retention even at elevated temperatures¹, while program/erase cycling shows strong endurance², and simple device structure enables high-density integration^{3,4}, making RRAM an attractive solution for embedded nonvolatile memory (eNVM). The RRAM properties, such as nonvolatile behavior, multilevel operation, and good scaling capability, align closely also with the requirements of various computing applications in image classification and voice recognition⁵. Despite its promising characteristics, RRAM technology still faces critical challenges in variability, which hinder its adoption as a mature embedded nonvolatile memory technology. While material and device engineering can partially address this issue by tuning oxygen non-stoichiometry of the switching layer⁶ to stabilize the filament dynamic or by doping the oxide to decrease the grain size⁷ and suppress the later diffusion⁸, the programming scheme also directly influences the evolution dynamics of conductive filaments and control switching behavior. Properly designed programming schemes can suppress abrupt switching behavior, reduce stochastic variations, and improve both switching uniformity⁹.

Generally, two operation modes of circuits are distinguished: voltage mode and current mode. In voltage mode, the programming voltage pulse is typically directly applied to the two-terminal RRAM device to modulate its resistance and achieve the target states. However, particularly during the SET operation, where a conductive filament changes the RRAM resistive state from high to low, to prevent the device from the potential damage caused by the abrupt increase of current, a current compliance is usually used to limit the maximum SET current. In two-terminal devices, this is typically achieved by external tools or passive elements such as resistors. With the development of two terminal RRAM cell to three terminal one-transistor-one-resistor (1T1R) structure, the external gate terminal of MOS transistor brings more possibility of RRAM programming in voltage mode, as the current compliance is obtained by applying a voltage to the gate of the transistor, which acts as a voltage controlled current

source. Advanced programming schemes as incremental step pulse with verify algorithm (ISPVA)¹⁰, incremental gate voltage with verify algorithm (IGVVA)¹¹ and dispersion aware program-verify algorithm (PVA)¹² are introduced into RRAM operation to optimize RRAM performance in multilevel programming for both information writing and storage as eNVM. It has been demonstrated that these programming schemes are capable of controlling the programmed conductance precisely. However, it should be noted that the verification of accurate programming with incremental pulse and conductance states can result in an increase in power consumption.

As for current mode, the current programming pulse¹³ (or sweep¹⁴) is generated by reference current source and directly fed to the RRAM device. Operating RRAM devices with current is quite promising to improve device performance in reliable resistance switching or better uniformity of low resistive states (LRS) distribution¹⁵. From the circuit design point of view, the reference current source could drive a broader range of loads in current mode, hence the switching process could be less influenced by the resistive change of RRAM and the related change of transistor working point¹⁶. Moreover, there is no need for setting an additional current compliance during SET operation, since the current is directly fed to the RRAM.

In this work, we propose a two current mirrors - one RRAM - one voltage buffer (2M1R1B) circuit to execute current programming of RRAM devices. By utilizing pairs of current mirrors to copy the current from a reference DC current source and chop transistors to shape the programming pulse, our proposed circuit aims at feeding well defined current programming pulses to RRAM devices. With DC measurements on SET and RESET branches in our circuits, we measure the mirror factor at various current amplitudes to evaluate its deviation from target factor 1.0 and the operation range by varying DC voltage supply of two branches. Moreover, mismatch of MOSFETs is characterized by evaluating the mirror factor deviation across the whole wafer. With transient characterization, we evaluate the mirror factors with pulses to assess the stability of mirroring action. Furthermore, by tuning the chop pulses' edge we characterized the mirror performance of our circuit at different time scale. Finally, we discuss the non idealities and possible improvement of our circuit to optimize current programming of RRAM.

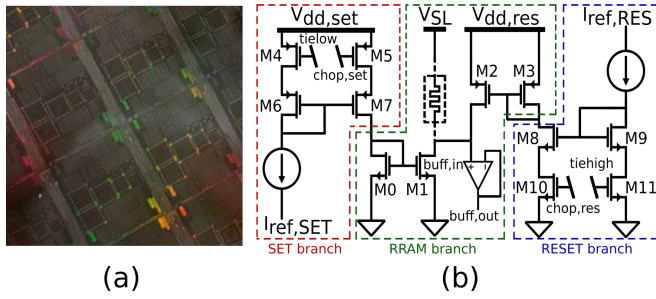


FIG. 1. (a) Photograph of the fabricated wafer containing multiple dies. (b) Schematic of the 2M1R1B circuit.

II. DESCRIPTION OF THE CIRCUIT

The proposed circuit, designed in a standard 180 nm technology node, is shown in Fig. 1. Figure 1a shows the taped-out wafer that includes our circuit, whereas its schematic is sketched in Fig. 1b. The circuit is divided in three main branches: SET branch, RESET branch, and RRAM branch. The set branch, shown in red dashed line, generates current pulses to switch the RRAM to its SET state. Two p-type metal-oxide-semiconductor (PMOS) devices, M4 and M5, are used as chopping switches to convert a DC current, $I_{ref,set}$, into a current pulse. The gate terminal of M4 is always grounded to provide a large voltage, $V_{dd,set}$, across its source-gate voltage and keep M4 in the deep-triode region with a $V_{SD,M4}=0$ V. Therefore, when a negative large voltage pulse, from $V_{dd,set}$ to 0 V, is applied to the gate of the counterpart device, M5, the source-drain voltage of M5, $V_{SD,M5}$, will immediately tend to zero to keep M5 in the deep-triode region for the duration of the input voltage pulse. In case of ideal symmetry, both M4 and M5 will show the same small resistances leading to a high matching between the devices of the p-channel current mirror, M6:M7, which increases the accuracy of the mirroring process. Next, as long as the input voltage pulse is active, a current as large as the reference current, $I_{ref,set}$, is mirrored into the output of the set circuit, M0:M1, producing a current pulse for the duration of the input voltage pulse. The generated negative current pulse mirroring into the RRAM branch, shown in green dashed line, switches the RRAM, and the voltage across the RRAM is measured by a voltage buffer.

Regarding the RESET circuit, shown in blue dashed line, a similar strategy is employed by which the RRAM can be reset in current mode. Briefly, the gate of M11 is always connected to additional DC supply, V_{dd} to keep M11 in deep-triode region and as soon as a positive voltage pulse, from 0 V to V_{dd} , is applied to the gate of its counterpart device, M10, the DC reference current ($I_{ref,res}$) is mirrored into the output of the reset circuit by current mirror M9:M8. Thus, for duration of the input voltage pulse, a current pulse with an amplitude of $I_{ref,res}$ is generated by which the RRAM is sourced through current mirror M3:M2. In this work, voltage sensing is used to read the exact resistance of the RRAM by draining read current pulse to RRAM to evaluate its LRS or high resistive state (HRS) status.

III. RESULTS

A. DC characterization

To verify the circuit's performance, DC measurements are performed on SET as well as RESET branches first.

In the DC measurements on the SET branch, the reference current $I_{ref,set}$ is programmed from 50 μ A up to 450 μ A as DC input of the PMOS mirror (M6:M7). The power supply $V_{dd,set}$ is set at 5 V, and the mirrored current is also read from same terminal by subtracting the reference current. Moreover, the second power supply is used to provide common ground for the circuit. The corresponding mirrored current and the mirror factor are shown in Fig. 2. As the reference current is increased, the mirrored current in branch M5/M7/M0 exhibits a linear relationship. The mirror factor is typically maintained at approximately 1.0 across the entire current range. Nonetheless, a departure from the optimal ratio of 1.0 persists in the lower current range, with a maximum aberration of 3% observed at 50 μ A. This current mismatch could be ascribed to the voltage mismatch of M6:M7. In SET branch, M4 and M5 are in the deep triode region during the operation to provide a matching of $V_{s,M6}$ and $V_{s,M7}$. But the node $V_{d,M7}$ is affected by the $V_{dd,set}$, while $V_{d,M6}$ is regulated by current source. While operating small current with a high voltage supply of $V_{dd,set}$, the node $V_{d,M7}$ could be pulled up to higher voltage by $V_{dd,set}$, which leads to a higher mirroring current.

After characterizing the mirror factor, we assess the operating range of our circuit by sweeping $V_{dd,set}$ from 0 to 5 V. Same as previous measurement, the mirrored current is read from the power supply by subtracting the reference current. The voltage level of the $V_{chop,set}$ is established 0 V to maintain a matching of M4:M5. The reference current has been set to 400 μ A. The relationship between the measured current and the $V_{dd,set}$ is illustrated in Fig. 3. The minimum $V_{dd,set}$ required by the SET branch is approximately 3.5 V to mirror the reference DC current. With the further decreasing of $V_{dd,set}$ to 2 V, the mirror current drops gradually, which is caused by the voltage mismatch of V_{sd} of M6:M7. Once the $V_{dd,set}$ is lower than 2 V, the current source can not maintain the DC current output under low voltage supply, which results in a fast current drop to zero.

As in the case with DC measurements performed on the SET branch, the mirror factor and operation range of $V_{dd,res}$ are characterized on the RESET branch. The reference current $I_{ref,set}$ is programmed from 50 μ A up to 450 μ A as DC input of the n-type metal-oxide-semiconductor (NMOS) mirror (M8:M9). The power supply $V_{dd,res}$ is set to 5 V, and the mirrored current is also read from the power supply terminal. Same as the prior measurement configuration, the shared ground is furnished by the extra power supply. The mirror factor is characterized in the first instance. The corresponding mirrored current and the mirror factor are displayed in Fig. 4. The mirror current and the reference current exhibit a linear relationship. The mirror factor is mainly maintained at approximately 1.0 across the whole operation current range. As was the case in the SET branch, in the lower current range there is a deviation observed, with a maximum 6% at 50 μ A.

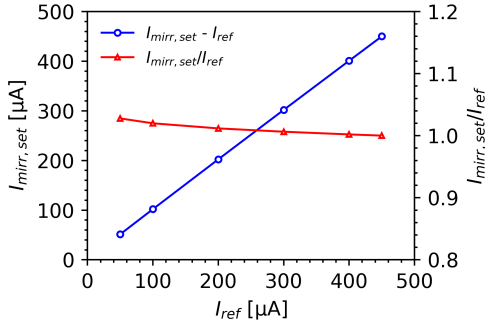


FIG. 2. DC characterization of the mirror in the SET branch. The mirrored current $I_{\text{mirr,set}}$ in branch M5/M7/M0 increases linearly with $I_{\text{ref,set}}$ varying from 50 μA to 450 μA (blue curve). The corresponding mirror factor across the whole $I_{\text{ref,set}}$ is kept approximately at 1.0 (red curve) with a maximum aberration of 3% at 50 μA .

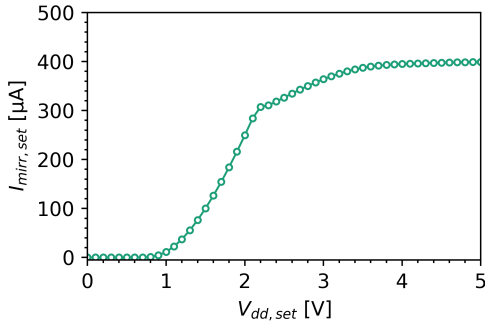


FIG. 3. Operation range assessment of SET branch with DC measurement. $I_{\text{mirr,set}}$ is measured while sweeping $V_{\text{dd,set}}$ from 0 V to 5 V with $V_{\text{chop,set}}$ at 0 V.

As discussed in the previous measurement, the voltage mismatch of M8:M9 could cause this deviation while operating in the low current range. In RESET branch, M10 and M11 are in the deep triode region during the operation to provide a matching of $V_{\text{s,M8}}$ and $V_{\text{s,M9}}$. Since all transistors are NMOS, $V_{\text{s,M8}}$ and $V_{\text{s,M9}}$ are actually pulled down to zero. In this case, the $V_{\text{ds,M8}}$ is more sensitive to the mismatch of $V_{\text{d,M8}}$, especially when this branch is operated with lower current.

Following the mirror factor characterization, the characterization of operation range of $V_{\text{dd,res}}$ is performed on the RESET branch. The power supply is swept from 0 to 5 V while concurrently measuring the current. The $V_{\text{chop,res}}$ is set to 5 V to maintain a high matching of M10:M11. The reference current is still set to 400 μA . In Figure 5, the relationship between the current and $V_{\text{dd,res}}$ is demonstrated. The measured current is the precise value of the mirrored current in branch M3/M8/M10. According to the $V_{\text{chop,res}}$ values, the voltage supply can be lowered down to 4 V without affecting the normal operation of the circuit. A comparison of the two branches reveals that the operation range of general voltage supply in the RESET branch is narrower than the SET branch. The origin of this minimum voltage supply difference could be the diode connected transistors M0 and M3. As introduced in previous sections, transistors M4 and M5 as well as M10

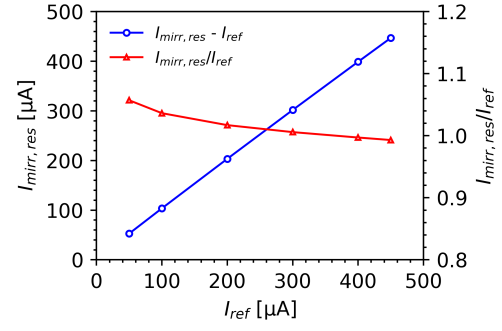


FIG. 4. DC characterization of the mirror in the RESET branch. The mirrored current $I_{\text{mirr,res}}$ in branch M3/M8/M10 increases linearly with $I_{\text{ref,res}}$ varying from 50 μA to 450 μA (blue curve). The corresponding mirror factor across the whole $I_{\text{ref,res}}$ is kept approximately at 1.0 (red curve) with a maximum aberration 6% at 50 μA .

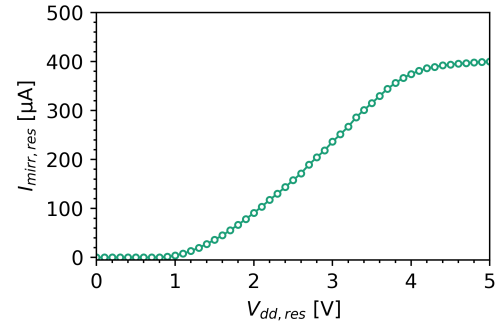


FIG. 5. Operation range assessment of RESET branch with DC measurement. $I_{\text{mirr,res}}$ is measured while sweeping $V_{\text{dd,res}}$ from 0 V to 5 V with $V_{\text{chop,res}}$ at 5 V.

and M11 are all operated in deep triode region. In the case of ideal matching, they can pull the source voltage of mirror M6:M7 as well as M8:M9 to power supply and ground. For these two pairs of current mirrors, the diode connected gate voltages are controlled by the current source. In this configuration the diode connected NMOS M0 and PMOS M3 are affected by the power supply. However, for p-channel transistor, due to the lower carrier mobility, it required larger gate source voltage to carry the same amount current as n-channel transistor. Furthermore, in the diode connected configuration, the gate source voltage is equal to drain source voltage. Thus, the diode connected M3 needs a larger drain-source voltage than M0.

To evaluate the impact of process variation as well as complementary metal-oxide-semiconductor (CMOS) mismatch on uniformity of average mirroring accuracy on wafer scale, DC measurements are performed on 180 dies of the wafer. For each die, two 2M1R1B circuits at different position of the die are measured with four reference current from 100 μA to 400 μA . And later the mean mirror factor of these four current values of each test circuit on each die is calculated. The average mirroring accuracy of both branches at wafer level are shown in Fig. 6 and Fig. 7 in the form of heatmap. The SET branch shows a homogeneous distribution of mirror fac-

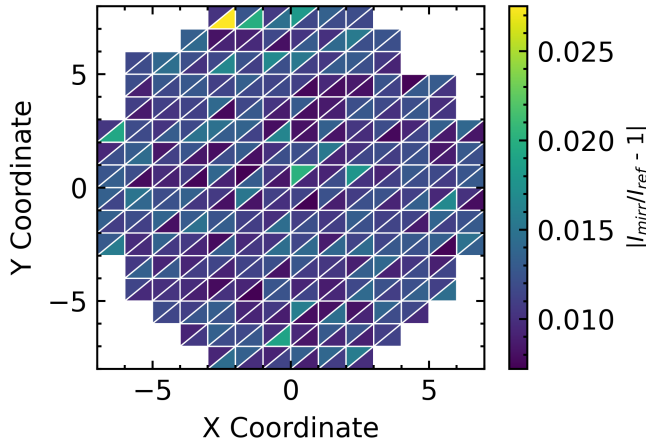


FIG. 6. CMOS mismatch evaluation of SET branch at wafer level with DC measurement on two same 2M1R1B structures per die.

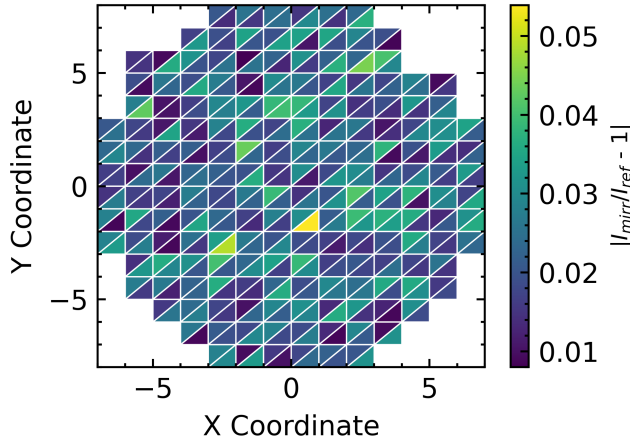


FIG. 7. CMOS mismatch evaluation of RESET branch at wafer level with DC measurement on two same 2M1R1B structures per die.

tor deviation in the range of 1% to 2%, besides one circuit on the first intensively tested die. As for the RESET branch, the mirror factor deviation is in the range of 1% to 4% with several 2M1R1B structures from different dies show highest deviation in the middle of wafer. Since the RESET process of RRAM operation has a higher robustness on current than SET operation, the deviation is acceptable. Compared to the RESET branch, the average mirroring accuracy of SET branch is less influenced by process variation and CMOS mismatch, which is crucial to program RRAM to different LRS states with precise current control during the operation. As for RESET branch, even with deviation up to 4%, it is still able to mirror enough current to reset the device.

B. Transient measurement

To characterize the circuit's performance under the pulse operation, transient measurements are performed on SET as well as RESET branches.

The performance of SET branch in transient operation is firstly evaluated by executing following set of measurements on silicon. With varying the reference current value, the mirror factor can be calculated by reading the amplitude of corresponding current pulses. Furthermore, with set of different rise time of the chop pulse, the edge of current pulse can be verified. The mirror factor of PMOS current mirror M6:M7 is firstly measured. In this case, the current source is programmed to generated DC current from $50\ \mu\text{A}$ up to $400\ \mu\text{A}$. As mentioned perviously in Section 2, a negative large voltage pulse, from $V_{\text{dd,set}}$ to 0, is applied to the gate of M5 in a waveform with period $20\ \mu\text{s}$ and rise time $1\ \mu\text{s}$ as well as duration time $10\ \mu\text{s}$. The corresponding $V_{\text{dd,set}}$ is setup to DC 5 V and later changed to 4 V as in DC measurement to evaluate the mirror properties under lower operation voltage. After all input signal setup, the mirror current is collected at source of M0 and measured by oscilloscope with an input resistance $50\ \Omega$. Each different measurement is repeated 50 times and averaged to minimize the influence of the noise coming from the setup on the measurements.

The characterization results are shown in Fig. 8. All current pulses are characterized with sharp pulse edge with $1\ \mu\text{s}$ rise time and $10\ \mu\text{s}$ duration. The current pulse waveform basically matches our chop pulse's waveform. At the end of pulse rising edge, the slope of the pulse edge becomes gradual, which indicates a well current controlling of our circuit. In the duration region, although the signal is noisy, the average of amplitude of each current pulse basically match its reference value from $50\ \mu\text{A}$ to $400\ \mu\text{A}$, which basically covers our target RRAM operation current range. To further evaluate the PMOS current mirror's functionality, we compare the mean value of $I_{\text{mirr,set}}$ with I_{ref} and further calculate the mirror factor as shown in Fig. 9. Same as DC characterization, there is a clear quasi linear relation between $I_{\text{mirr,set}}$ and I_{ref} and the overall mirroring factor in reference current range ($50\ \mu\text{A}$ to $400\ \mu\text{A}$) is mainly maintained at approximately 1.0 across the whole operation current range with a maximum of 2% at $400\ \mu\text{A}$. Both current pulses' waveform in Fig. 8 and the less deviated average mirror factor indicate that the SET branch is able to convert the DC reference to pulse by chopping operation and there is no impactful parasitic capacitance observed in the converted current pulse, which is usually characterized by spikes at the end of pulse rising edge. To exam the mirroring accuracy under lower power consumption, $V_{\text{dd,set}}$ is lower to 4 V. As the orange curve shown in Fig. 9 the mirror current drop in the range of $300\ \mu\text{A}$ to $400\ \mu\text{A}$ with a maximum 7% at $400\ \mu\text{A}$. However, in the lower current range from $50\ \mu\text{A}$ to $200\ \mu\text{A}$, the mirror factor shows a small deviation less than 3%, which brings possibility to program RRAM with small current to further lower the power consumption.

Additionally, the SET branch as a current pulse generator, its ability to generate a current pulse with a waveform defined by the $V_{\text{chop,set}}$ is important to the further RRAM programming, where the filament evolution during SET is influenced by the current. To do this, the chop pulse with rise time from $100\ \text{ns}$ to $1\ \mu\text{s}$, meanwhile keep the duration time at $10\ \mu\text{s}$ and period at $20\ \mu\text{s}$. At the mean while, $V_{\text{dd,set}}$ is set to 5 V to provide enough power supply to drive the current. The final mea-

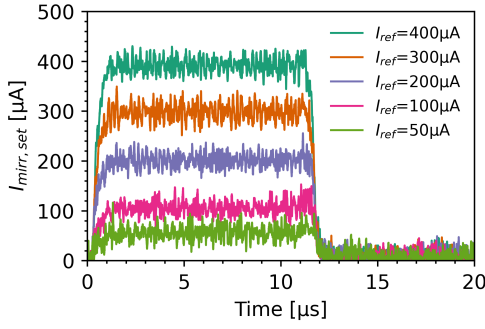


FIG. 8. The average of 50 mirrored current pulses with I_{ref} ranging from 50 μA to 400 μA measured from transient measurements on the SET branch.

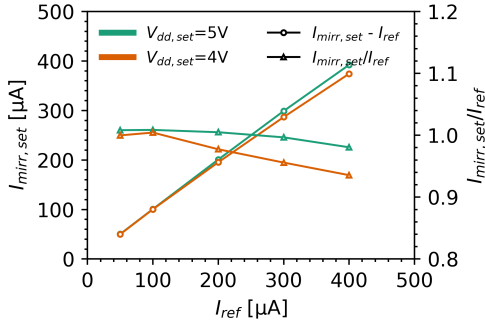


FIG. 9. $I_{mirr,set} - I_{ref}$ relation and corresponding mirror factors with I_{ref} ranging from 50 μA to 400 μA under variable $V_{dd,set}$.

measurements' results are shown in Fig. 10. To further observe and compare current pulse edge, the time scale is converted to log scale. The edge of each current pulse is in the corresponding time scale from 200 ns up to 1 μs , which is comparable to the chop pulse. And later this current pulse will be further mirrored to the RRAM branch to SET the device, which aims at studying the SET dynamic of RRAM in current programming mode. However, in the case of rise time at 100 ns, there is a small platform observed at the rising edge. One of the possible explanation is that the signal is reflected in the waveguide. When the circuit is operated with maximum frequency 10 MHz, the probe as well as cables behave as waveguide. All cables have impedance of 50 Ω , but the metal pads are not exactly same as cables. As a result of this impedance mismatch, the signal could be reflected in the waveguide.

The performance of RESET branch in transient operation is further evaluated with set of measurements executed on silicon. The mirror current value is mainly discussed in this part, since the amount of current it can drive is the main concern for RESET operation of RRAM. Same as SET transient measurement, the current source is programmed to generated DC current from 50 μA up to 400 μA . Two power supplies are used to set $V_{dd,res}$ to 5 V and common ground for the circuit. $V_{chop,res}$ is programmed to positive large voltage pulse, from 0 to $V_{dd,res}$, is applied to the gate of M10 in a waveform with period 20 μs and rise time 1 μs as well as duration time 10 μs .

The mirror factor is firstly characterized and calculated in

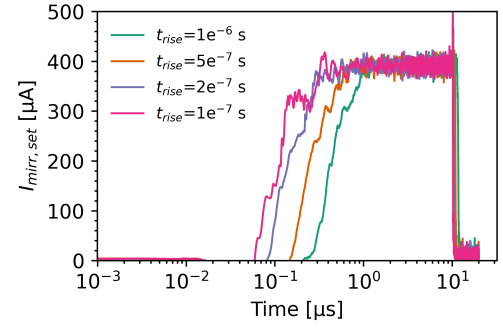


FIG. 10. The average of 50 mirrored current pulses with an I_{ref} of 400 μA and variable chop pulse edges ranging from 100 ns to 1 μs obtained from transient measurements on the SET branch. The time axis is on a log scale.

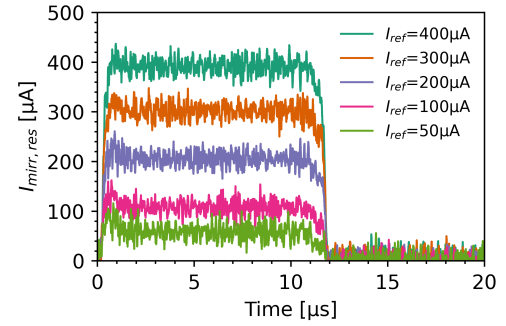


FIG. 11. The average of 50 mirrored current pulses with I_{ref} ranging from 50 μA to 400 μA measured from transient measurements on the RESET branch.

Fig. 12. Current pulses' waveforms comparable with SET branch are observable. The waveform of the generated current pulse at each DC reference value match the chop pulse in pulse rising as well as falling edge and duration time. The average pulse amplitude matches its reference value. However, there is a current overshoot observed at the rising edge of the generated pulse. This could be related to the parasitic capacitance. Further, the $I_{mirr,res} - I_{ref}$ relation curve as well as mirror factor are plotted and analyzed. As shown in Fig. 12, $I_{mirr,res}$ follows I_{ref} linearly same trend as observed in DC measurement. There is a deviation of the mirror factor observed in the low current range with maximum 7% at 100 μA . Overall, the RESET branch is able to generate current pulses across the targeting operation range as a good base for providing enough power to reset RRAM in the low current range.

As for RRAM branch, due to the lack of the device, the characterization of this branch mainly relies on the voltage buffer. By measuring the voltage at the input node of the buffer, we can briefly validate the sub branch M2/M1 as well as voltage buffer. To read the input node voltage properly, both M1 and M2 need to be operated in saturation, where both SET and RESET branches are required to be activated. In our case, both $V_{dd,set}$ as well as $V_{dd,res}$ are set to 5 V. Reference DC current source in both branches are programmed to 100 μA . By activating chop transistors M5 and M10 at same time,

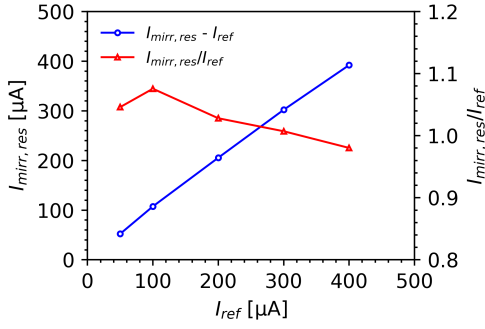


FIG. 12. $I_{\text{mirr,res}} - I_{\text{ref}}$ relation and corresponding mirror factors with I_{ref} ranging from $50 \mu\text{A}$ to $400 \mu\text{A}$ under fixed $V_{\text{dd,res}}$ of 5V .

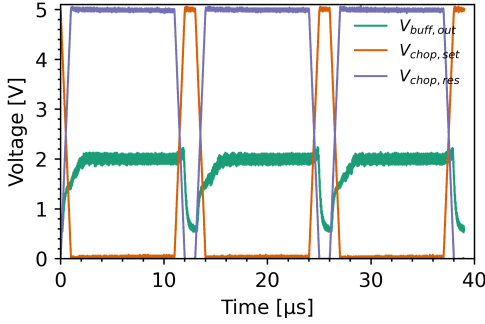


FIG. 13. The buffer read out voltage with applying both $V_{\text{chop,set}}$ and $V_{\text{chop,res}}$ synchronously. The delay time between pulses is set to $1 \mu\text{s}$ to avoid the parasitic capacitance introduced by floating bottom electrode.

two branches carry the generated current pulses to the RRAM branch, which leads to the self-regulation of M1 and M2 with proper gate voltage as well as drain voltage. Furthermore, the voltage buffer is activated with V_{tail} at 1V and V_{dd} 5V and the input node voltage change ($V_{\text{D,M1}}$ and $V_{\text{D,M1}}$) is read from buffer output connected to the oscilloscope shown in Fig. 13. It can be observed that read-out voltage $V_{\text{buff,out}}$ increases with applying chop pulses. It researches a stable read-out value around 2V within the duration of chop pulses. Later read-out voltage decreases gradually with falling of chop pulses. It needs to be noticed that the read-out voltage falls down to 0.6V . This can be addressed to the parasitic capacitance in the branch M2/M1 introduced by the metal pad for RRAM bottom electrode deposition. The measured $V_{\text{buff,out}}$ reflects the conductivity of RRAM branch and functionality of designed voltage buffer. Moreover, since NMOS M1 and PMOS M2 in series, to carry same amount current in saturation, the overdrive of M2 should be around $1.4 - 1.7$ times larger than M1, which match our measurement result, where the absolute value of M2's drain source voltage is 3V .

IV. DISCUSSION

The proposed 2M1R1B structure is used to execute current programming of RRAM. From the device engineering point

of view, the measurement results discussed previously is adequate for our purposes. From DC measurements, SET branch is able to mirror current comparable to the reference value with less than 3% deviation. This accurate mirroring current will be further copied to RRAM by mirror M0:M1 to program the device in current mode without any extra current compliance implementation. The transient measurement's result indicates that the generated current pulse matches the chop pulse well in pulse's waveform. Moreover, the generated current pulse increases gradually at the end of its rising edge rather than overshoot spike caused by parasitic capacitance in 1T1R structure under the voltage mode. All these features indicate that our proposed 2M1R1B circuit has a well control of the generated current pulse. As a result, the SET programming of RRAM can benefit from this well defined current pulse in better control of filament dynamic. During the SET process, oxygen vacancies' drift under the electrical filed contributes to the ionic current of the whole SET current. With a accurate control of SET current, it would be possible to control the filament evolution during SET precisely and increase the switching uniformity. Furthermore, the accurate mirroring current amplitude brings the flexibility to do multi-level programming within a low current range rather than carefully choosing gate voltage for the transistor as current compliance in 1T1R structure. With the symmetric design of the SET branch, the RESET branch is also able to generate current pulses within our targeting current range, which brings the possibility to explore the RESET process of RRAM with current programming. Additionally, our proposed 2M1R1B circuit is able to read-out the conductance of the RRAM cell with voltage sensing mode by measuring the voltage drop over the cell with constant read current pulse through the voltage buffer. When extended to array level, from the crossbar array programming point of view, the voltage sensing mode used in our approach can lower the power consumption during vector matrix multiplication (VMM) by applying small constant read current. And the sensed voltage cross the cell can be further accumulated and directly processed by the analog-to-digital converter (ADC), which could prevent the large consumption of power and area peripheral circuits to sink large current while clamping voltage⁵.

From the circuit design point of view, 2M1R1B circuit can be further optimized. As introduced in Fig. 1(b), current mirrors in RRAM branch are implemented with basic current mirror topography with same width over length (W/L) ratio of MOSFETs to get 1:1 mirror factor. With neglect of channel-length modulation and current mirror working in the saturation, the copied current has no dependence on V_{ds} and it is only influenced by the W/L ratio of implemented MOSFETs as it can be seen from the following equation:

$$\frac{I_{D1}}{I_{D0}} = \frac{\frac{1}{2}\mu_n C_{\text{ox}} \left(\frac{W_1}{L_1}\right) (V_{\text{GS0}} - V_{\text{TH}})^2}{\frac{1}{2}\mu_n C_{\text{ox}} \left(\frac{W_0}{L_0}\right) (V_{\text{GS1}} - V_{\text{TH}})^2} = \left(\frac{W_1}{L_1}\right) \left(\frac{W_0}{L_0}\right)^{-1} \quad (1)$$

where μ_n is the mobility of charge carriers, C_{OX} is the gate-oxide capacitance per unit area, V_{TH} is the threshold voltage,

W_0 and W_1 refer to the gate width of M0 and M1, and L_0 as well as L_1 refer to the gate length of M0 and M1. As a result, the reference current pulse can be well mirrored to RRAM. However, in practice, channel-length modulation of MOSFET causes errors in copying current as it can be seen from the following equation:

$$\begin{aligned} \frac{I_{D1}}{I_{D0}} &= \frac{\frac{1}{2}\mu_n C_{ox} \left(\frac{W_1}{L_1}\right) (V_{GS1} - V_{TH})^2 (1 + \lambda V_{DS1})}{\frac{1}{2}\mu_n C_{ox} \left(\frac{W_0}{L_0}\right) (V_{GS0} - V_{TH})^2 (1 + \lambda V_{DS0})} \\ &= \frac{W_1 L_0}{W_0 L_1} \cdot \frac{1 + \lambda V_{DS1}}{1 + \lambda V_{DS0}} \end{aligned} \quad (2)$$

where λ is the channel-length modulation coefficient. While $V_{DS0}=V_{GS0}=V_{GS1}$, V_{DS1} may not be equal to V_{GS1} because of the circuitry fed by M1, which is the RRAM cell. During the SET process, the voltage divider between RRAM and transistor is changed, which leads to a variation of V_{ds} of transistor. Moreover, due to device to device variability, V_{ds} mismatch is more difficult to minimize. In order to minimize the influence of channel-length modulation, several circuit topologies can be employed. The initial approach involves the implementation of a cascode topology, which serves to shield the current source and thereby mitigate the voltage variation across it¹⁷. In practice, as a transform of basic cascode mirror, the configuration "low-voltage cascode" is widely used to reduce voltage supply, which is common issue when designing with cascode structure. Comparing to the basic current mirror, cascode or even low-voltage cascode current mirror can minimize the voltage mismatch.

V. CONCLUSION

In this work, we proposed and designed a circuit to program RRAM with current pulses. Thanks to the current mirror topology, defined current can be copied to RRAM branch and hence SET process is more controlled and less influenced by the overshoot caused by parasitic capacitance from transistor. By characterizing the circuit in silicon, we demonstrated that our current generator circuit is adequate to execute current programming of RRAM.

ACKNOWLEDGMENTS

This work was supported by the European Research Council (ERC) through the European's Union Horizon Europe Research and Innovation Programme under Grant Agreement No 101042585. Views and opinions expressed are however those of the authors only and do not necessarily reflect those of the European Union or the European Research Council. Neither the European Union nor the granting authority can be held responsible for them. The University of Groningen would

like to acknowledge the financial support of the CogniGron research center and the Ubbo Emmius Fund.

DATA AVAILABILITY STATEMENT

The data that support the findings of this study are available from the corresponding author upon reasonable request.

- ¹H. Suga, H. Suzuki, Y. Shinomura, S. Kashiwabara, K. Tsukagoshi, T. Shimizu, and Y. Naitoh, "Highly stable, extremely high-temperature, nonvolatile memory based on resistance switching in polycrystalline pt nanogaps," *Scientific reports* **6**, 34961 (2016).
- ²J. J. Yang, M.-X. Zhang, J. P. Strachan, F. Miao, M. D. Pickett, R. D. Kelley, G. Medeiros-Ribeiro, and R. S. Williams, "High switching endurance in taox memristive devices," *Applied Physics Letters* **97** (2010).
- ³J. Y. Seok, S. J. Song, J. H. Yoon, K. J. Yoon, T. H. Park, D. E. Kwon, H. Lim, G. H. Kim, D. S. Jeong, and C. S. Hwang, "A review of three-dimensional resistive switching cross-bar array memories from the integration and materials property points of view," *Advanced Functional Materials* **24**, 5316–5339 (2014).
- ⁴D. Bridarolli, F. Carletti, S. Ricci, M. Porzani, P. Mannocci, M. Farronato, and D. Ielmini, "3d vertical resistive random-access memory (3d-vrram) for analog in-memory computing," in *2025 Non-Volatile Memory Technology Symposium (NVMTS)* (2025) pp. 1–4.
- ⁵W. Wan, R. Kubendran, C. Schaefer, S. B. Eryilmaz, W. Zhang, D. Wu, S. Deiss, P. Raina, H. Qian, B. Gao, *et al.*, "A compute-in-memory chip based on resistive random-access memory," *Nature* **608**, 504–512 (2022).
- ⁶K. Skaja, M. Andr a, V. Rana, R. Waser, R. Dittmann, and C. Baeumer, "Reduction of the forming voltage through tailored oxygen non-stoichiometry in tantalum oxide rram devices," *Scientific reports* **8**, 10861 (2018).
- ⁷K. Lee, Y. Kim, H. Na, and H. Sohn, "Effect of aliovalent impurities on the resistance switching characteristics of sputtered hafnium oxide films," *Journal of Vacuum Science & Technology B* **33** (2015).
- ⁸H. He, X. Yuan, W. Wu, C. Lee, Y. Zhao, and Z. Liu, "Impact of al alloying/doping on the performance optimization of hfo2-based rram," *Electronics* **13**, 2384 (2024).
- ⁹H. Lim, W. Shim, and T.-H. Kim, "Impact of reset pulse width on gradual conductance programming in al2o3/tiox-based rram," *Micromachines* **16**, 718 (2025).
- ¹⁰E. P rez, A. J. P rez- vila, R. Romero-Zaliz, M. K. Mahadevaiah, E. P rez-Bosch Quesada, J. B. Rold n, F. Jim nez-Molinos, and C. Wenger, "Optimization of multi-level operation in rram arrays for in-memory computing," *Electronics* **10**, 1084 (2021).
- ¹¹V. Milo, F. Anzalone, C. Zambelli, E. P rez, M. K. Mahadevaiah,  . G. Ossorio, P. Olivo, C. Wenger, and D. Ielmini, "Optimized programming algorithms for multilevel rram in hardware neural networks," in *2021 IEEE International Reliability Physics Symposium (IRPS)* (IEEE, 2021) pp. 1–6.
- ¹²F. M. Puglisi, C. Wenger, and P. Pavan, "A novel program-verify algorithm for multi-bit operation in hfo2 rram," *IEEE Electron Device Letters* **36**, 1030–1032 (2015).
- ¹³P. Jain, U. Arslan, M. Sekhar, B. C. Lin, L. Wei, T. Sahu, J. Alzate-vinasco, A. Vangapaty, M. Meterelliyoz, N. Strutt, A. B. Chen, P. Hentges, P. A. Quintero, C. Connor, O. Golonzka, K. Fischer, and F. Hamzaoglu, "'13.2 a 3.6mb 10.1mb/mm² embedded non-volatile rram macro in 22nm finfet technology with adaptive forming/set/reset schemes yielding down to 0.5v with sensing time of 5ns at 0.7v,'" in *2019 IEEE International Solid-State Circuits Conference - (ISSCC)* (2019) pp. 212–214.
- ¹⁴L. WT, L. YT, *et al.*, "Improved resistive switching uniformity in cu/hfo2/pt devices by using current sweeping mode," (2011).
- ¹⁵B. Gao, W. Y. Chang, B. Sun, H. W. Zhang, L. F. Liu, X. Y. Liu, R. Q. Han, T. B. Wu, and J. F. Kang, "Identification and application of current compliance failure phenomenon in rram device," in *Proceedings of 2010 International Symposium on VLSI Technology, System and Application* (2010) pp. 144–145.
- ¹⁶X. Liu, C. Bengel, F. C ppers, O. Solfronk, B. Zhang, S. Hoffmann-Eifert, S. Menzel, R. Waser, and S. Wiefels, "Effect of transistor transfer characteristics on the programming process in 1t1r configuration," *IEEE Transactions on Electron Devices* **71**, 2423–2430 (2024).
- ¹⁷B. Razavi, "Design of analog cmos integrated circuits," , 5:139–145.